

Soft pneumatic actuator-driven origami-inspired modular robotic “pneumagami”

The International Journal of
Robotics Research
2021, Vol. 40(1) 72–85
© The Author(s) 2020
Article reuse guidelines:
sagepub.com/journals-permissions
DOI: 10.1177/0278364920909905
journals.sagepub.com/home/ijr


Matthew A Robertson¹, Ozdemir Can Kara² and Jamie Paik

Abstract

This article presents a new modular robotic platform for enabling reconfigurable, actively controlled, high-degree-of-freedom (high-DoF) systems with compact form factor. The robotic modules exploit the advantages of origami-inspired construction methods and materials, and soft pneumatic actuators (SPAs) to achieve an actuator embedded, parallel kinematic mechanism with three independently controlled “waterbomb” base legs. The multi-material, layer-fabricated body of the modules features selectively compliant flexure hinge elements between rigid panels that define the module as a kinematic 6R spherical joint. The precision layer-fabrication technique is also used to form embedded distribution channels within the module base to connect actuators to onboard control hardware. A decentralized control architecture is applied by integrating each module with small-scale solenoid valves, communication electronics, and sensors. This design approach enables a single pneumatic supply line to be shared between modules, while still allowing independent control of each leg joint, driven by soft, inflatable pouch actuators. A passive pneumatic relay is also designed and incorporated in each module to leverage the coupled, inverted inflation, and exhaust states between antagonistic actuator pairs allowing both to be controlled by a single solenoid valve. A prototype module is presented as the first demonstration of integrated modular origami and SPA design, or pneumagami, which allows predefined kinematic structural mechanisms to locally prescribe specific motions by active effect, not just through passive compliance, to dictate task space and motion. The design strategy facilitates the composition of lightweight, high-strength robotic structures with many DoFs that will benefit various fields such as wearable robotics.

Keywords

Modular robots, reconfigurable robots, layer fabrication, origami robots, parallel kinematics, continuum robots, diaphragm actuators, soft pneumatic actuators, soft robots

1. Introduction

New methods, materials, and manufacturing techniques are recently redefining the field of robotics with regard not only to expanding the diversity of practical applications, but also toward improving the capabilities of new systems. In particular, these new developments complement the demands of a quickly growing area of interest within the robotics community, in wearable devices. Prior work has demonstrated the potential for wearable robotics, through applications targeting rehabilitation, augmentation, and assistive support (Al-Fahaam et al., 2016; Huo et al., 2016; In et al., 2015; Polygerinos et al., 2015; Robertson and Paik, 2016). Although some of these provide ready solutions to a narrow scope of problems confined to fixed settings owing to their reliance on tethers for offboard power and control, the extended prospect of such technology is its application to mobile or daily use. In order to achieve more

practical systems that can be applied to more general activities of daily living (ADLs) in the real world, the challenges of human–robot interaction and wearability for various applications motivates the design of new systems that are concurrently portable, safe, reconfigurable, and with high degrees of freedom (DoFs) to meet diverse needs.

In recent years, a new type of wearable device has been explored that can be operated as an additional (third) arm or appendage to enhance the manipulation capabilities and

Reconfigurable Robotics Laboratory (RRL), Institute of Mechanical Engineering, School of Engineering, Ecole Polytechnique Federale de Lausanne, Lausanne, Switzerland

Corresponding author:

Jamie Paik, Reconfigurable Robotics Laboratory (RRL), Institute of Mechanical Engineering, School of Engineering, Ecole Polytechnique Federale de Lausanne, Lausanne, Switzerland.
Email: jamie.paik@epfl.ch

dexterity of a human user by providing task assistance. Supernumerary robotic limbs (Davenport et al., 2012), composed of a backpack and two 3-DoF arms, have been developed to aid a wearer in tasks that require stabilization and positioning. Similar in terms of scale and weight, a 3-DoF wearable robotic forearm has also been proposed for the needs of construction workers (Vatsal and Hoffman, 2017). Soft robotic systems offer a convenient alternative to these in terms of lower weight and smaller scale, as well as implicit safety for human–robot interactive related tasks. The common form of soft robotic solutions is a monolithic body (Cianchetti et al., 2012; Kurumaya et al., 2018; Liang et al., 2018; McMahan et al., 2005; Qi et al., 2017; Renda et al., 2014; Yang et al., 2018), however soft poly limbs have been proposed as a system of exchangeable limbs that can be mounted on different parts of the human according to various tasks (Nguyen et al., 2019).

To achieve a similar type of wearable assistive device with high mobility, but significantly lower size and weight for less-demanding tasks, an origami-inspired robotics design approach presents advantages over previous device design and fabrication methods. Utilizing nominally 2D components to achieve complex, active and passive 3D structures (Onal et al., 2011; Paik et al., 2012), this design framework naturally affords compact physical form factors in robotics, yielding systems that are lightweight, scalable, easy to store and transport, and conducive to rapid, low-cost, mass manufacturing, and even self-assembly (Felton et al., 2015, 2014; Tolley et al., 2014, 2013). Leveraging these benefits, origami design methods have thereby been employed to create various types of mobile robots (Lee et al., 2013; Miyashita et al., 2015; Onal et al., 2013; Vander Hoff et al., 2014; Zhakypov et al., 2015), deployable structures (Kim et al., 2018), biomedical devices (Salerno et al., 2016), manipulators, (Mintchev et al., 2018; Zhakypov et al., 2018; Zhang et al., 2016), and other mechanisms (Rodriguez Leal and Dai, 2007). The range and extensibility in terms of performance and DoFs across these examples highlight the versatility enabled by the origami design approach, which represents a promising strategy for implementing new wearable and human-interactive devices.

The robotic origami concept is adaptable to producing robots from many different materials, for both structural and active elements, and from a variety of fabrication techniques (Rus and Tolley, 2018). Passive kinematic structures are formed by combining rigid-body elements with compliant hinge joints (similar to the many folds utilized in traditional paper origami) to create reconfigurable, virtually soft, yet strong assemblies capable of supporting loads. The generally planar components can be cut from thin sheet materials such as cardboard, glass-fiber composites, or plastics, often using a CNC laser. Alternately, origami designs can be easily implemented by 3D printing (Ge et al., 2014; Liu et al., 2018). Flexible hinge joint elements between rigid-body components can either be combined as a separate layer bonded to the planar (commonly Kapton

polyimide), unfolded form of the origami structure, or directly through 3D printing with soft materials.

Similar to the assembly of different passive layers in robotic origami, actuator elements can also be directly incorporated in the layered structures to provide joint motion and stiffening (Firouzeh and Paik, 2017), and to create fully integrated robotic origami structures (Firouzeh and Paik, 2015). This previous work has successfully demonstrated shape memory alloy (SMA) and shape memory polymer (SMP) layers in integrated robotic origami designs, although a variety of other actuation techniques have also been investigated, including the use of anisotropic heating (Na et al., 2015), fluid absorption (Mu et al., 2015), dielectric elastomers (Ahmed et al., 2014), piezoelectric actuators (McClintock et al., 2018), and magnetics (Salerno et al., 2017). While these embedded actuator solutions provide robotic origami structures with controllable shape changing abilities, the practical utility of such systems is generally restricted owing to their limited force and power output. Soft pneumatic actuators (SPAs) offer both a high power-to-weight ratio as well as an implicitly safe alternative source of actuation through the use of flexible and compliant materials (Polygerinos et al., 2017). Moreover, owing to their generally simple construction, SPAs can be customized by design and operation at various supply pressures to match the scale of assistance needed for wearable assistive devices (Robertson et al., 2017). The integration of pneumatic systems and SPAs with origami-inspired structures, however, remains a significant challenge as they are generally non-compatible with the style of layer manufacturing employed. One promising exception to this is the pouch-type SPA, which is layer fabricated from plastic sheets and has been shown to be directly compatible with origami topology (Niiyama et al., 2014). Nevertheless, a complex, high-DoF robotic system composed of origami-based structures and powered by SPAs has not been shown as a consequence of other open challenges such as the need for embedded pneumatic power distribution and decentralized control.

Origami-based robotic continuum structures have been developed in previous work that utilized tendon cable transmission for actuation. One such example employs water-bomb pattern origami structures to create a continuum robot morphology driven by three tendon cables (Zhang et al., 2016). The cable actuation method complicates the control of a multi-DoF arm, however, and limits the workspace as every module and DoF is mechanically coupled together. Other work has addressed these limitations by incorporating truly modular units that can be serially combined to form a robotic arm structure, with onboard DC motors which drive internal cables to allow independent control of each of the modules 3 DoFs (Santoso et al., 2017). These modules use a different, Yoshimura origami pattern structure that also allows bending and contraction or extension range of motion (RoM). In both examples of prior work, however, neither utilize the origami-inspired

structure for more than kinematic constraint to afford torsional rigidity in resistance to bending in unwanted directions or to provide restoration force to oppose contractile cable tension. This latter attribute means that the modules or complete robotic assembly can only be actuated in one direction (cable tension), while only an elastic restoration force is available to act against antagonistic loads. Furthermore, while these designs utilize 2D fabrication techniques to produce the origami-inspired structural elements, these are incorporated and assembled with other components following inherently traditional methods.

Following a modular design approach leveraging the benefits and design methods of the previously described modular pneumatic (Robertson and Paik, 2017) and modular origami (Belke and Paik, 2017) systems, we present a novel platform which consists of a multi-functional origami-inspired structure, low-profile soft pneumatic pouch actuators, and embedded networking hardware for enabling reconfigurable, actively controlled, high-DoF soft systems with a compact form factor (Figure 1).

This pneumatically powered origami, or pneumagami, module is constructed from a 3-DoF waterbomb pattern which constrains the kinematic workspace to three independent joint angles for controlling the module platform angle and linear displacement. With a pair of antagonistic pouch SPAs controlling each of these joints, the module is fully controllable. To enable manufacturing ease and scalability, the module as a whole is principally designed to allow complete fabrication and assembly using 2D and layer manufacturing techniques, with minimal added components. Consequently, the presented module employs a dual-function main body structure which contains embedded air distribution channels to serve as an active manifold, connecting all onboard pneumatic components and supply lines. In addition, a layer-fabricated pneumatic relay element is designed and implemented to simplify the control of antagonistic actuators and minimize weight. The multi-functional use of the origami body structure and integration of other functional components amenable to 2D manufacturing techniques is a unique method of constructing an embedded system that can be applied to a diverse range of robotic morphologies. This novel approach allows us to conceive a system-level design and configuration of the origami structure both in kinematic and dynamic dimensions, applied here to realize compact and lightweight multi-DoF, pneumatically powered modules.

The main contributions of this section are:

- the first example of the design and fabrication of an integrated robotic module that combines both origami-inspired structures and pneumatic actuation (pneumagami);
- implementation and characterization of the multi-DoF pneumagami module and a novel differential pressure blow-off relay (DBR) valve for underactuated control;
- establishing a framework for future research in developing compact, customizable wearable devices for task assistance.

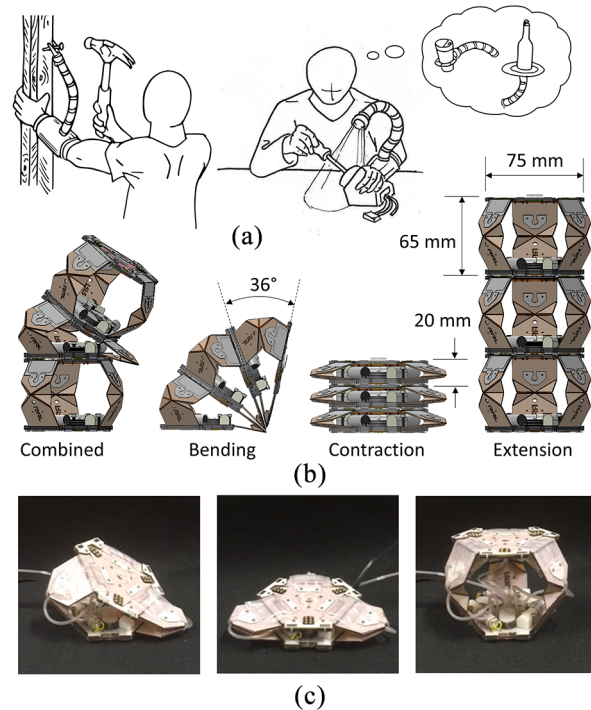


Fig. 1. A pneumagami-based modular robotic system. Lightweight, high-strength, and compact pneumagami modules hold potential to enable new forms of wearable robotic devices for general task assistance in daily activities (a). With three independently controlled DoFs and high RoM in both angular bending and linear motion (b), the modules can be reconfigured to suit a variety of objectives. A physical prototype module is implemented and shown in (c).

2. Design

A pneumagami module consists of an origami-inspired structure, soft pneumatic pouch actuators (pouch SPAs), and embedded power and control components. The onboard hardware allows multiple modules to be connected in series with independent control over every powered DoF (three antagonistic joint pairs, with two actuators each), while allowing only single lines to be used for pneumatic power distribution, forward control signals, and inertial measurement unit (IMU) sensor feedback between the modules. This efficient architecture enables the assembly of large networks of modules, including a linear arrangement to form a continuum-style robotic manipulator arm.

2.1. Functional origami-based integrated structure

A preliminary objective of the module structure is to achieve 3-DoF spherical RoM with high performance in a compact, low-mass form factor, as one potential purpose for the modules is for use in portable robotic systems. These requirements motivate the use of origami-inspired

design, materials, and fabrication methods for the frame. Following this approach, a classical origami pattern known as the waterbomb is used to create a spherical joint with 2D rigid plate structures connected by 1-DoF hinge joints in place of folds. A waterbomb-based parallel kinematic design for the module is employed to enable 3-DoF motion of a moving upper platform. When produced using sufficiently thin body plates and sufficiently wide flexure-based joint hinges, this structure furthermore facilitates collapsibility, allowing the module to be folded down to a predominantly flat shape roughly 11 mm in thickness from a fully extended height of 50 mm.

The structure of a module is composed of three main components: a lower base section, an upper moving platform, and three waterbomb pattern linkages (legs). The complete module frame is formed by connecting the lower and upper platforms by the legs. This parallel kinematic arrangement allows the upper platform to move relative to the lower platform through a spherical workspace, as well in linear displacement.

The kinematic origami frame serves several important purposes. The primary role is to simply join the mobile segments of the module through linkages that allow high RoM as desired, and limited mobility otherwise. The parallel configuration of the waterbomb legs produces many coupled DoFs, which provides that the angular position and location of the upper platform is geometrically defined by only three independent variables. This allows the structure to be physically reconfigured by controlling the actuation of only three joints to set the platform to a new position and orientation. In this manner, the frame consequently acts as a functional component, as part of the mechanical work transmission from actuators to final output.

The origami frame also plays an important role in increasing the overall stiffness of the multi-DoF module. Although the structure features three independent DoFs, its mobility is not infinite. One significant constraint is preserved through the use of the hinge-jointed waterbomb linkages, which acts to restrict any torsional motion on the axis normal to either platform. This results in a structure that is fully controllable in all its allowable DoFs, and rigid in all others to the limit of its component material stiffness. In a robotic arm configuration, with a large serial continuum assembly of modules, this torsion constraint acts to resist passive “off-axis” deformations. In typical soft robotic systems that rely on compliant materials for their primary structure and actuation, such uncontrolled deformations reduce the stiffness of the overall system and yield to bending in cantilevered or overhanging orientations (such as reaching tasks).

The origami frame is fabricated in two main parts, with the majority and largest part formed by a single, monolithic base structure that is folded into its final shape. This base structure (seen in Figure 2), contains the lower base platform connected to each of the three legs that are fabricated together from 2D glass-fiber sheets and kapton polyimide layers. The central base platform not only joins the legs

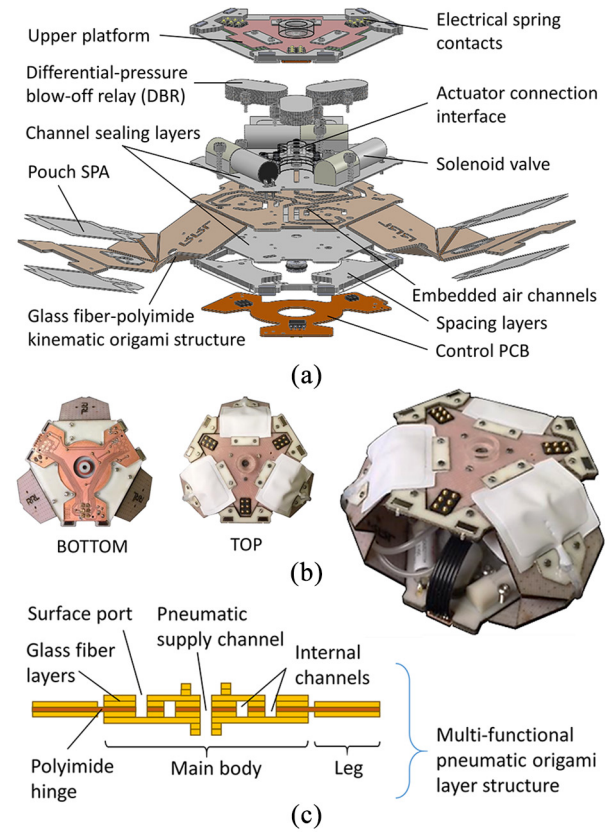


Fig. 2. An exploded view of the pneumagami module CAD model is shown in (a), while the actual prototype in the fully assembled and complete state can be seen in (b). The layer-fabricated structure of the module serves dual purposes, as both parallel kinematic spherical linkage and a functional supply pressure distribution manifold used to connect onboard pneumatic components (c).

together, but like the kinematic mechanism formed by the legs, it also serves additional multipurpose function. While the rigid components of the legs are formed by solid plates consisting of a central kapton hinge layer sandwiched between two glass fiber layers (three layers total), the base structure is extended by an additional two glass-fiber layers above and below the layers common to the leg structures. The common layers in the base structure are then manufactured with open channels that are sealed by the outer glass-fiber layers to form an embedded network within the platform for pneumatic power distribution. The topside layer (on the inside of the complete module) contains port holes for interfacing control valves, relays, supply lines, and actuators with the embedded layer-manufactured distribution manifold.

2.2. Pouch actuators

To actively change configuration, the modules are powered by soft, nominally flat, low-profile pneumatic pouch actuators that are form compatible (nominally 2D) with the

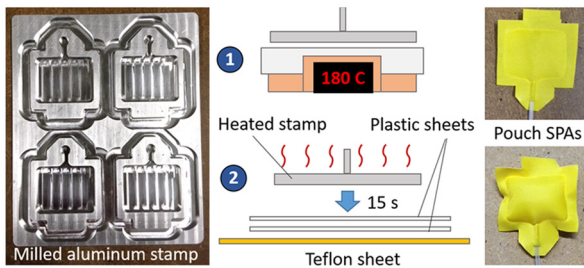


Fig. 3. Pouch SPAs used to drive the module legs are fabricated from plastic sheets, sealed by heat using a machined aluminum stamp. The resulting actuators are high strength, being driven at up to 60 kPa pressure, lightweight, and extremely thin and flexible.

origami structural frame. Each actuator is fabricated from polyethylene or PEVA plastic sheets material, heat and pressure bonded together with a custom-made stamp. The CNC machined aluminum stamp is heated on a hot plate to 180°C, and then transferred and pressed by hand onto two plastic sheets placed on a Teflon surface for 15 seconds. The extruded stamp makes contact with the sheets which fuse to form a sealed contour around an unsealed inner chamber. The inner volume of the actuator is inflated through an inlet neck where small pneumatic supply tubing can be inserted. The fabrication process and photos of the aluminum stamp and produced SPAs can be seen in Figure 3.

The pouch SPAs are used to actuate the three joints that connect the legs to the upper platform, although the respective joints fixed to the base structure could also be used instead. Two actuators are located at each joint around the platform, with one on the inner (lower) and one on the outer (upper) sides of the joint. Each actuator is positioned across the joint at the center, and mechanically fixed at two opposing ends with mounting screws to the two rigid bodies of the joint, the platform and leg section. When inflated, the pouch actuators exert a tensile force between the two end attachment points, as well as a compression force imparted at the joint center itself, which both act to decrease the joint angle on the side of the actuator.

The two actuators on either side of the upper leg joints act antagonistically to drive the joint in both directions, however they cannot be independently controlled. Rather, the states of the antagonistic actuator pairs are coupled such that one of the two actuators is always active. This design was chosen for several reasons. For one, this provides controllability and module stiffness at all times. Being fabricated from thin plastic, the pouch SPAs provide no stiffness or structural support when not active, and the origami kinematic structure itself provides only very light passive stiffness from the bending of very thin (50 μm) flexure hinge joints. In this way, the structure is very susceptible to deformations caused by external loads. Although a larger spring

element could be included to replace the second antagonistic actuator, the force or torque provided by this spring is passive and fixed by a constant displacement relationship, limiting its ability to counteract loads. Furthermore, the active joint actuator would need to provide additional power to overcome both the spring stiffness and any driven load. This requires a stronger actuator, and yields a less-efficient system. By coupling the actuator states, the module does not rely on passive stiffness to recover its joint configuration, and active control can be applied in both directions to ensure full authority.

The bidirectional joint control is inversely coupled to also reduce the number of required solenoid valves needed to activate each pouch SPA (six in total). In order to achieve modularity, this decentralized control hardware is built into each module and thereby contributes to the overall size and mass of the module itself, which has a direct effect on its performance. When multiple modules are assembled in a serial configuration, as with a manipulator arm, every attached module imposes a load on its preceding module. In an effort to maximize the work output of such a multi-module configuration, the size and weight of every module can be significantly reduced by minimizing the number of valves onboard. This strategy of controlling coupled states in two actuators with a single control valve is common in industrial pneumatic systems where 5/2 valves, 5 ports with 2 states, are used. At small scales, this type of valve is not common however. Instead, we employ a novel solution inspired by industrial pneumatic logic control systems, which allows two actuators to be controlled by a single common 3/2 port solenoid valve in combination with a custom-designed, layer-fabricated passive relay valve.

2.3. Pneumatic relay

In the most common pneumatic system set-up, actuators are typically individually controlled by 3/2 port solenoid valves. This type of valve has two states, in which a common port is either connected to a pressurized supply port or to an exhaust port. The common port is usually then connected to the actuator to be controlled, thereby switching between providing pneumatic power to the actuator, or allowing air in the actuator to vent back through the valve and exhaust port. In an alternate configuration that is seldom used, the pressurized supply can be connected to the common port, allowing the two valve states to switch between providing supply pressure to either of the other two ports. In principle, this allows both states of a single valve to be used to supply pressure to two different outputs. In practice however, this is impractical on its own since actuators cannot vent themselves, so would never be able to release the pressure supplied in this manner after a single use. The solution to operating two actuators with a single valve is to use a different type of valve, with 5 ports which

allow simultaneous venting inversely coupled to the activation of both output ports, however this style valve is currently unavailable at the scale of the pneumagami module.

In order to control the antagonistic pouch SPAs integrated with the pneumagami module, we leverage the two states of a single small-scale 3/2 valve by incorporating a custom-designed and layer-fabricated DBR. Although two DBR components are required to pair with each solenoid valve for controlling two coupled actuators, the combination occupies less volume with lower mass than two active solenoid valves. The key principle of this device is that it utilizes the pressure supplied to one actuator to trigger a mechanical vent which allows the opposite SPA to release its pneumatic pressure. This thereby facilitates control of two actuators connected through a 3/2 valve in common supply orientation. When an actuator is connected to the supply and activated in one state, it is correspondingly disconnected from the supply and vented to atmosphere in the other state, and vice versa for its antagonistic pair. This process is depicted in Figure 4.

2.3.1. Relay operating principle. The operation of the DBR follows a simple force-balance relationship, induced by pressure and a bias spring. The free body force equation for the internal moving poppet is represented by

$$PA_p + F_k + PA_d = 0 \quad (1)$$

where A_p is the area of the poppet upper side, F_k is the force from the bias spring, and A_d is the area of the diaphragm below the poppet.

The DBR contains two control ports, a high and low side, and one vent chamber. The high side is exposed to the upper side of the poppet, whereas the low side allows pressure to flow to the diaphragm. The vent is nominally isolated from the high and low side ports of the device owing to a bias spring that holds a poppet closed. When opened, the poppet allows airflow from the high side of the DBR to the vent, however the low side remains isolated at all times by a non-permeable but flexible diaphragm. A single actuator is simultaneously connected to the opposite sides of two different relays, as well as one side of the control solenoid valve. When one actuator is active (A-1), the high side of one relay (DBR-1) is pressurized forcing the poppet and vent to close. At the same time, the low side of the other relay (DBR-2) is pressurized, which causes a flexible diaphragm to displace upward, pushing directly on the bottom side of the internal poppet seal. Since the area of the diaphragm exceeds that of the top side of the poppet, the net force from equal pressure on both sides force the poppet up. Once open, the pressure on the high side of DBR-2 is relieved through the vent. The steady conditions in this state are DBR-1:closed and DBR-2:open. Once the solenoid valve state is switched, the process reverses. The other actuator A-2, the high side of DBR-2, and the low side of DBR-1 are connected to the supply pressure. This closes the DBR-2 poppet, and again, while pressure

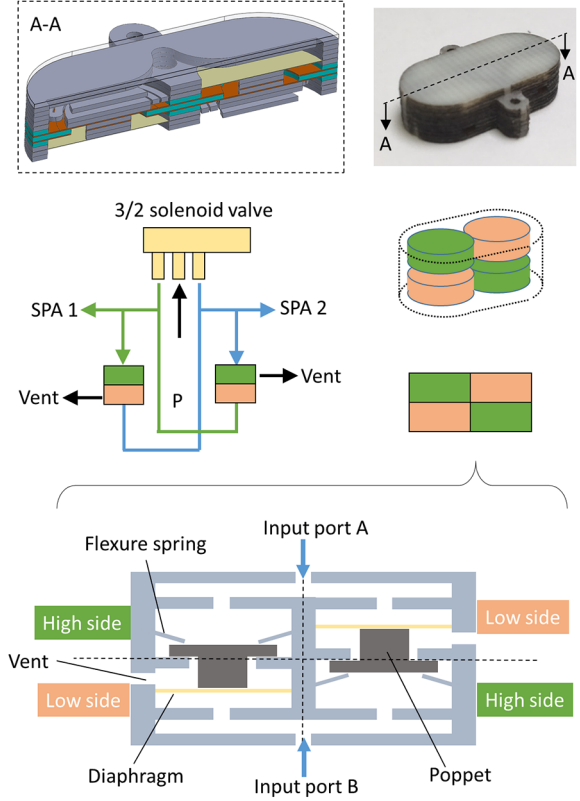


Fig. 4. Diagram of a DBR valve.

remains in A-1 and on the high side of DBR-1, the larger diaphragm area pressurized by the same source causes the poppet to move upward and the vent in DBR-1 to open, exhausting pressure in A-1.

2.4. Embedded control hardware

Each pneumagami module contains embedded hardware that allows it to be connected together directly with other modules and reconfigured in a “plug-n-play” manner to form larger robotic systems. To enable this functionality, a printed circuit board (PCB) is integrated in each module with electronics for communication and control of the onboard solenoid valves. Activation signals to the valves are routed through an integrated circuit (IC) on the PCB over a common, single wire control bus that is shared among all connected modules. The IC (WS2811) decodes the position ID of the module as well as the independent actuator channel within the module. In addition to forward control signals, feedback from an IMU on the PCB can be accessed through a two wire I²C interface that is also shared among all connected modules in a system assembly.

3. Experiments

3.1. Linear stiffness

The linear stiffness of the module was tested in the vertical direction using a stress-strain material testing system

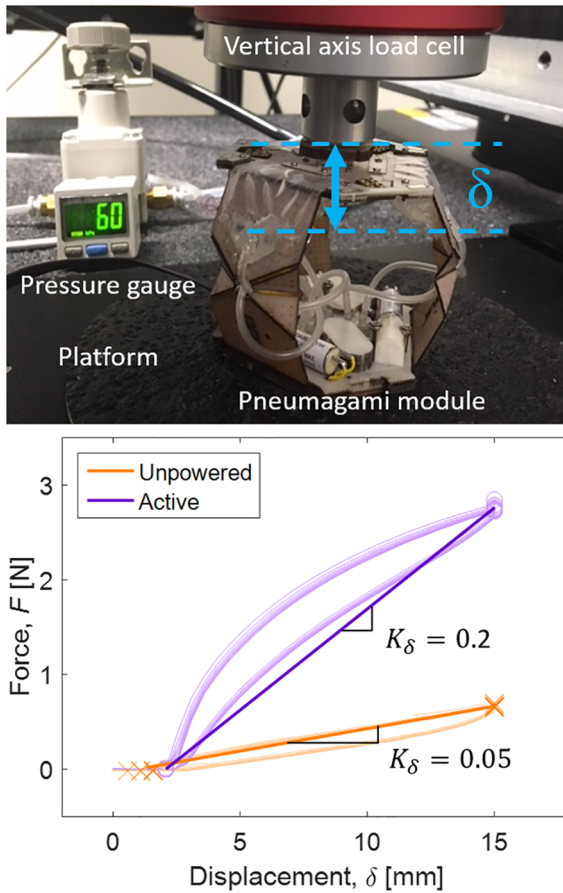


Fig. 5. Experimental setup for performing linear stiffness measurement tests with the module in powered (SPAs pressurized) and unpowered (SPAs deflated) states using a vertically oriented material testing system.

(Instron 5965). For each test the module was placed on the rigid base of the testing machine directly below the load cell attached to the movable linear stage. The load cell was initialized to zero force and displacement just after contact with the top of the module, and the force and displacement were then recorded for ten cycles of downward deflection, $\delta = 15$ mm. The module was tested in two configurations: unpowered and powered. In the first condition, only the passive stiffness of the polyimide joints as well as tubing connecting the upper and lower stages of the module contributed to the stiffness. In the second condition, the pouch SPAs in all three legs were activated with a supply pressure of 60 kPa to force the upper module platform up vertically to its maximum position. The results of the two linear force–displacement tests are seen in Table 1 and can be in Figure 5, where the active linear stiffness is shown at $K_\delta = 0.2$ to be a factor of 4 times greater than the passive linear stiffness at $K_\delta = 0.05$. In the active state, the increase in stiffness is a direct effect of the pouch SPAs stiffening from pneumatic inflation, and is therefore not a fixed value, but dependent on the supply pressure.

3.2. Passive torsional stiffness

The torsional stiffness of the origami structure was measured in a torque–angular displacement setup. An unpowered module was fixed in a horizontal position at the base to a rigid structure while the upper platform of the module was attached to a freely rotating torque arm. The torque arm is constrained by a shaft aligned with the axial center of the tested module, and extends to a length of 100 mm where it is terminated by a rounded endpoint feature. The same vertical materials testing machine was used to apply a load on the end of the torque arm, while the rounded shape of the arm endpoint helps to ensure that the load is transmitted at the same distance for small displacements through the flat contact surface protruding from the load cell.

Although the module test setup was fixed in place relative to the load cell and only linear force and displacements were measured directly, a corresponding torque applied to the module and resulting angular displacement were calculated from the known geometry of the setup, neglecting the effects of load redirection at relatively small angular deflections. For each measurement trial, a linear deflection of 2 mm was prescribed corresponding to less than 1.2° of angular rotation.

Two trials of 10 cycles each were performed to test the torsional stiffness of the modules in two different configurations: fully extended and fully collapsed. The raw and averaged results of the experimental tests are shown in Figure 6, which indicate a value of higher stiffness in the compact state compared with the extended state. This result follows the reasoning that in the contracted state, the flexible cross joints at the center of each leg are positioned radially further from the axial center of applied torque and resulting rotation of the upper and lower module platforms, where the force on each flexure hinge joint is therefore reduced. In the extended state, as the legs straighten and intermediate hinge joints move closer to the axis of applied moment, the resulting force acting through the legs on the joint is greater, resulting in higher off axis deflection of the flexible hinge material and a lower measured torsional stiffness.

3.3. Actuator and relay valve characterization

A single module leg was fabricated to test the step response of antagonistic pouch actuators, as well as characterize the observed delay effect of the DBR. The test leg comprises a single joint fabricated to the same specifications and material as those found in the legs of the complete module. Two pouch SPAs are mounted on either side of the leg hinge in an antagonistic configuration as seen in Figure 7(a) and supplied with pneumatic pressure from independent supply tubes. With the leg fixed to a mounting structure, the actuators were activated at least 15 cycles in each direction to maximum deflection at 60 kPa, by two different control methods. In the first method depicted in Figure 7(b), two

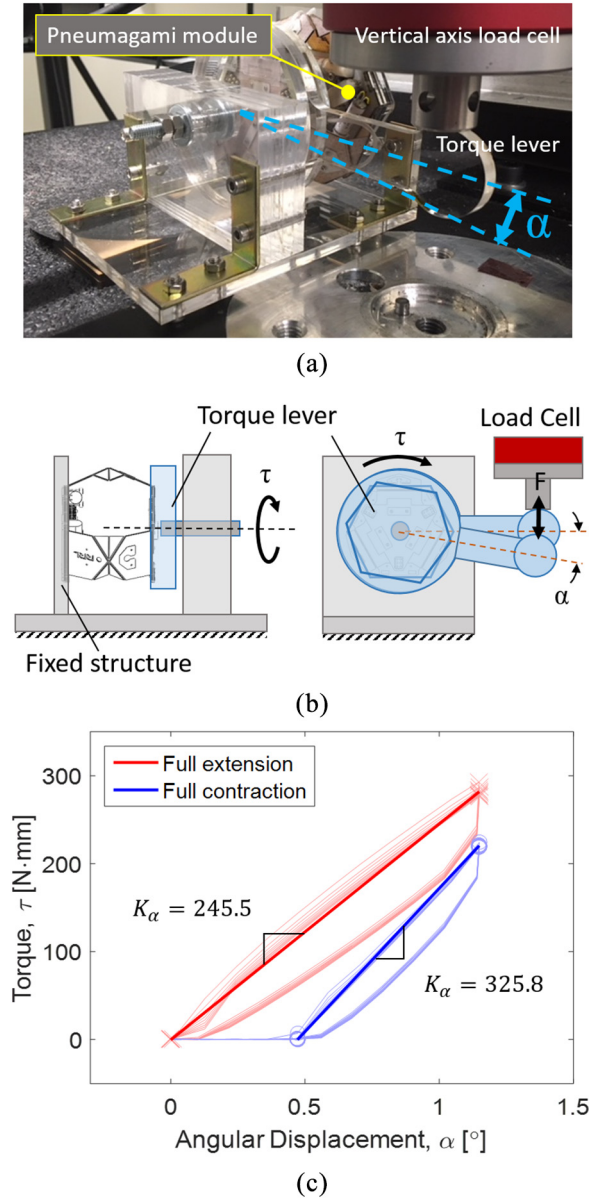


Fig. 6. The torsional stiffness of the pneumagami module was tested by applying a torque load to the upper platform of the module along its central axis while the lower base platform was fixed. A test setup was designed to transmit force from the linear material test machine into torque, while both the load and displacement were measured. The test rig includes a rotational shaft constraint to ensure that only pure moment is applied to the module without any orthogonal linear force.

independent solenoid valves were used to command the activation of the two SPAs in a periodic, alternating pattern. A digital pressure sensor (Honeywell, 001BGAA5) in parallel with each actuator recorded the changes in pressure resulting from the cyclic activation through an analog port of an Arduino microcontroller. The same test was then repeated using a single solenoid control valve coupled to the two ports of a DBR and each of the antagonistic SPAs, as seen in Figure 7(c).

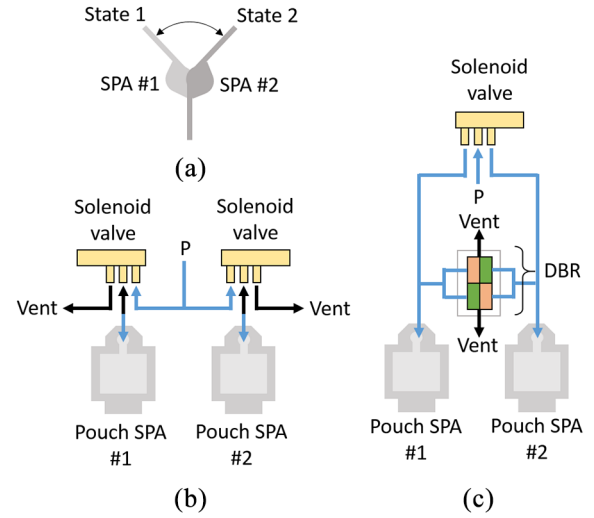


Fig. 7. The two configurations used for characterizing the DBR and actuator response to cyclic pressure step inputs are shown. The two states shown in (a) are achieved by alternating activation of antagonistic SPAs through two control configurations illustrated in (b) and (c).

The cyclic pressure profiles for each experiment were averaged for 15 cycles and can be seen in Figure 8. From these measurements, the 10–90% rise times from neutral to fully pressurized state are calculated yielding 0.041 seconds for SPA 1 and 0.031 seconds for SPA 2. The longer response time for SPA 1 can be attributed to a small leakage that is visible as a short duration drop in pressure visible in the recorded data.

The actuator pressure profiles for the second configuration controlled by a solenoid and DBR pair are seen in the lower plot of Figure 8, which indicates rise times of 0.18 and 0.094 for SPA 1 and SPA 2, respectively. While the leakage effect is also visible in SPA 1 as seen previously, another effect is introduced by the inclusion of the DBR component, seen as a momentary delay in the pressurization of the actuator as its antagonist is depressurized and the pressure in both actuators is roughly equal, leaving only the force imbalance on the internal poppet of the relay caused by asymmetric areas to drive state switch and fully vent the opposing SPA. Although different DBR geometries were not tested in this study, future work could investigate methods for reducing this momentary delay by optimizing the ratio of functional areas, and hence forces, acting on the relay poppet.

The difference in pressure profile timing can also be used to quantify the effect of the DBR valve in terms of its maximum operating bandwidth. Taking the difference between the rise time of SPA 2 (the best performing measured actuator, with no apparent leakage) in the two configurations, the added delay from the DBR is found to be 0.063 seconds. Taken to be a characteristic of the relay response time, this correlates to roughly 5.6 Hz bandwidth for the DBR.

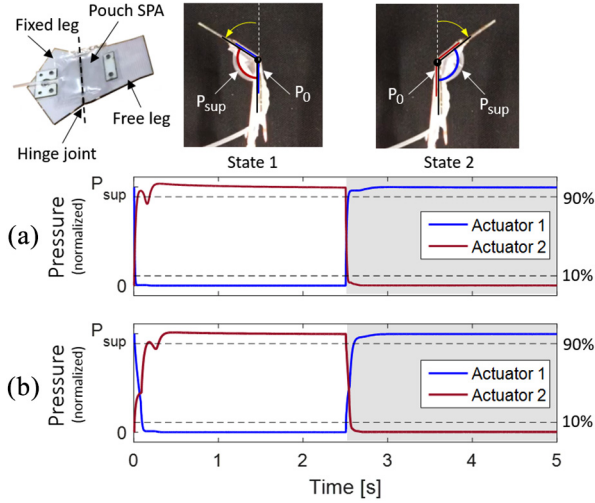


Fig. 8. Two averaged pressure profiles are shown for cyclic actuation of antagonistic SPAs fixed to an origami leg for joint characterization, corresponding to two different control methods. (a) The pressure profile associated with dual solenoid control. (b) The profile associated with single solenoid valve control utilizing a custom, layer fabricated DBR valve for state switching.

3.4. Kinematic model validation

The trajectory of the module upper platform angle, α , was tracked using the video analysis software Kinovea, and the result used to validate the applicability of an existing kinematic model for the waterbomb-based parallel structure to the prototype presented here. A video camera was placed above the complete 3-DoF module for testing and two markers in the plane of the platform rotation were tracked. The corresponding change in platform angle was computed based on the change in distance between the two points on the projected xy -plane (camera focal plane), as seen in Figure 9, following the geometrical relationship

$$\cos \beta_1 = \frac{d_1}{d_0} \quad (2)$$

Similarly, the leg angle trajectory was calculated from the measured position of a marker attached to the moving endpoint of one of the three legs, following

$$\cos \alpha = \frac{l_{leg} \cos \beta_0 + \delta}{l_{leg}} \quad (3)$$

where the initial leg angle, β_0 , and leg length, $l_{leg} = r_a$, were measured separately at the start of the experiment.

To validate the model, the platform angle trajectory was first recorded for seven cycles and averaged to produced a mean measured trajectory. The mean trajectory was then used as the input to the inverse kinematic model from Fang et al. (2013)

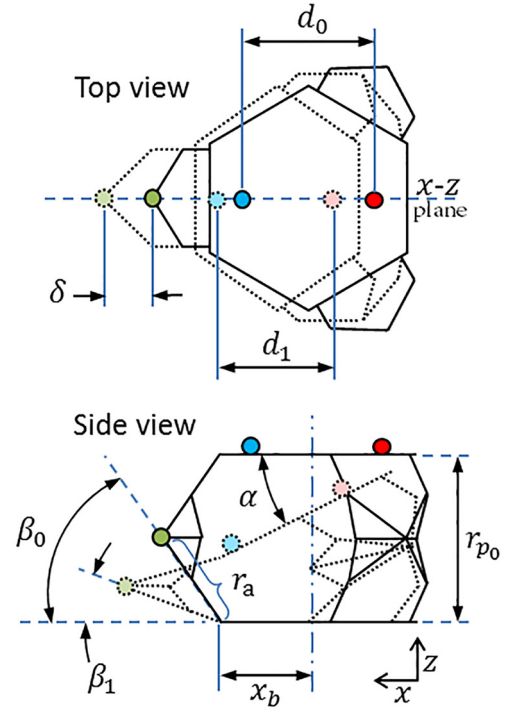


Fig. 9. Illustration of pneumagami module model and experimental setup. The pneumagami module is tested using attached markers viewed from above to track the angular displacement of a single leg, and the upper module platform. Relative motion of the markers in the camera focal plane is used to calculate the actual angular displacements.

$$\beta_1 = 2 \tan \left(\frac{-D_1 + \sqrt{D_1^2 - 4C_1E_1}}{2C_1} \right) \quad (4)$$

which is used to calculate leg joint angles β_i for given legs of the structure. For simplicity, this analysis considers only one leg, $i = 1$, however this model is derived in the original reference from which it is adapted specifically for multiple parallel origami-structured DoFs, and therefore directly applicable to the modules shown here.

For a single leg aligned with the global frame x -axis, $y_b = 0$, $\delta = 0$, $\phi = 0$, and $\psi = \alpha/2$, simplifying the coefficients to

$$\begin{aligned} C_1 &= r_p + 2x_b \sin \frac{\alpha}{2} - 2r_a \sin \frac{\alpha}{2} \\ D_1 &= 4r_a \cos \frac{\alpha}{2} \\ E_1 &= -r_p + 2x_b \sin \frac{\alpha}{2} + 2r_a \sin \frac{\alpha}{2} \end{aligned}$$

With the parameters of the given module $x_b = 25$, $r_p = 48$, and $r_a = 24.4$, the leg joint angle β_1 was calculated from the known upper platform angle trajectory. This theoretical result is then compared with the measured angle also

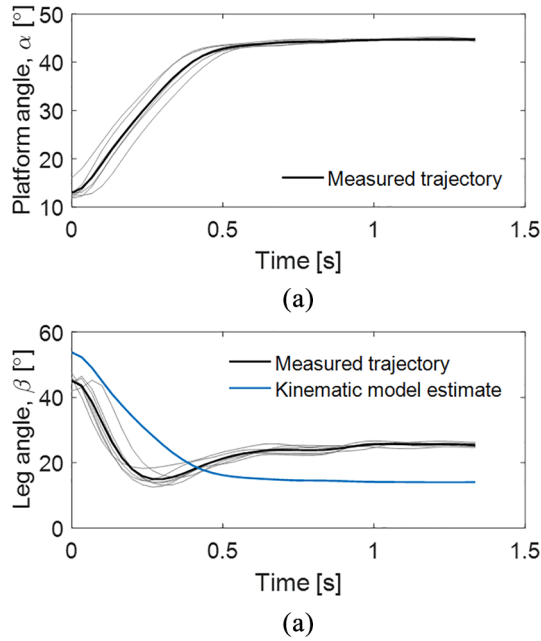


Fig. 10. The angular trajectory of the module upper platform is shown in (a), averaged from seven cyclic, binary activation of a single leg joint. An inverse kinematic model is used to calculate the theoretical trajectory of the activated leg joint, while the actual recorded measurements are shown for comparison.

measured through video analysis. Figure 10(a) shows the measured platform trajectory used as the independent variable above in (4). Figure 10(b) shows the predicted leg angle trajectory in comparison with the actual recorded trajectory. A general trend appears consistent between the two curves, however significant deviations are also clearly evident. The difference in the measured data to the theoretical model is likely due to at least two main factors: poor visual marker tracking which caused drifting in steady-state conditions, and perspective distortion resulting from markers moving vertically, out of the recording camera's focal plane.

In addition to measurement-based errors, the physical mechanics of the measured prototype may also contribute to differences between the theoretical and actual model trajectories. The leg angle trajectory shows two primary features that deviate from the model prediction, in a steady-state offset, and a transient overshoot. The first of these features may be the result of joint stiffness in the physical prototype that is not represented in the purely kinematic model. This stiffness in the non-activated legs of the physical module could act to constrain the upper platform vertically while still allowing significant radial motion resulting in greater angular deflection for a given joint angle. In this case, the joint angle of the activated prototype leg would not need to change as much as the model for a given platform angle, as it is shown by the higher angle offset. In addition, the non-idealistic mechanics of the prototype flexure joints may also have contributed to the overshoot in the

Table 1. Performance.

Property	Specification
Total mass	56 g
Valve mass (3)	4 g
DBR mass (3)	2.5 g
Contracted size	$65 \times 70 \times 20 \text{ mm}^3$
Extended size	$65 \times 70 \times 65 \text{ mm}^3$
Angular RoM	42.5°
Linear RoM	45 mm
Actuation speed	$81.6^\circ/\text{s}$
DBR bandwidth	5.6 Hz
Extended torsional stiffness	245.5 Nm°
Contracted torsional stiffness	325.8 Nm°
Active linear stiffness	0.2 N/mm
Passive linear stiffness	0.05 N/mm

leg joint angle that occurs approximately midway between the minimum and maximum platform angle, where the angular velocity of the platform is most likely to be changing direction. At this presumed inflection, play in the flexible joints of the leg may have allowed additional RoM in transience owing to inertial effects, that later settled with the joint at a higher angle in steady state.

4. Discussion

The position of three independent joint angles theoretically prescribe the final position of the pneumagami module platform, however, practical manufacturing and design differences from the physical module and the ideal model contribute to deviations in predicted performance. A prominent difference is the use of flexure-based joints in place of single-axis rotational joints throughout the structure. The polymer-based hinges produce a dominant mode of bending that can be approximated as a single axis, however multi-axis rotations and deformation of the compliant structure allows motion in other directions. This joint “play” allows deviation from pure rotational motion and idealized kinematics that would inhibit the application of model-based control methods for controlling this type of module to precise desired positions. This method of control is not necessarily needed or appropriate for this type of module however, owing to the intrinsic compliance of the pouch SPAs that are used to drive module joint motion. This intrinsic compliance allows the module to be physically adaptable to misalignment of the end effector relative to target positions. While this may not be the objective of every application for this type of module, the inherent compliance allows this actuator structure to be utilized in collaborative, wearable, or interactive applications to provide safe and compatible functionality.

The force output of the pneumagami module tested here is also comparable or lower than some existing origami modules designated for use in continuum robot arm structures; however, this is not a fundamental limitation of the design. The closest functional equivalent to the pneumagami architecture utilizes origami structure modules driven

by *onboard* DC electric motors to produce greater output force (Santoso et al., 2017). This design is most similar to the pneumagami concept because every DoF can be independently controlled utilizing motors that are located within each module, while drawing electrical power from an offboard source. This type of system is fundamentally limited by the coupling of motor size and weight to maximum output force or torque however, and since the motor is located onboard, the performance of the modules cannot be scaled without also scaling the size of the actuated modules. In this way, DC motor powered systems with independently controllable DoFs are not independently scalable in the way that pneumatically powered systems are. In contrast, pneumagami modules allow scalability of force output with no change in module or system scale and only minimal change in design through new materials and fabrication methods. As the modules are powered by pressurized air, the force output of the modules can be increased by increasing the supply pressure. While this may require the size and scale of the pump providing the pressure to also increase, this can be neglected as it is comparable in this analogy to the size of the electrical power supply in DC motor-based systems, which is not typically included when accounting for actuator mass or size. The actuators tested in this work were operated near the limit of the pouch SPAs before failure at their heat-fused edges, and from the plastic deformation of the plastic pouch material. The capacity of pouch SPAs to tolerate higher operating pressures and, thus, produce higher force output can be increased by utilizing stronger pouch materials and different methods for bonding the sealed structures. In addition, various adhesives and sheet composite types may be substituted to accommodate higher pressure in the embedded distribution manifold as well as to tolerate the higher forces in the kinematic structure. These design choices are seen as design parameters rather than fundamental limitations of the pneumagami concept, and allow the module design and performance to be scaled according to desired metrics.

Another type of origami-inspired continuum robot structure has been demonstrated utilizing *offboard* DC motors for actuation (Zhang et al., 2016). In this configuration, motors are used for driving a continuum of modules via tension cable *tendons* routed from a fixed base structure that houses the drive motors and any necessary transmissions or gearing. While this strategy enables high power-to-weight ratio actuation, it also imposes a practical limitation in scalability of system DoFs, in that each cable routed to control an independent DoF occupies finite space through the center axis of the continuum structure. A given space cannot accommodate many separate tendons, and therefore the system cannot be arbitrarily or independently scaled. This configuration also imposes performance limitations by introducing a mechanical coupling between all modules in series. Even in systems where adequate space allows every DoF to be independently controlled via tendons, the motion of any DoF in a tendon-driven system affects that of every other. This dependent actuation is very difficult to control.

Although a different kind of coupling exists through the pressure that drives pneumatically powered actuators in series, as it produces a pressure gradient along the length of a continuum of modules, this effect can be countered by the offboard power supply, preserving the scalability of pneumagami or other pneumatically actuated devices when the size of offboard components can be neglected. The coupling in purely mechanical, DC motor-driven systems cannot be eliminated or compensated directly by any means other than complex control (Camarillo et al., 2009), which accounts for the target orientation of all modules in series and adjusts the tension in all cables accordingly to isolate and execute a particular DoF actuation.

The onboard, embedded control hardware allows multiple modules to be connected directly in series with each other to form a hyper-redundant manipulator arm in the simplest multi-module form. The modules are not limited to use in this configuration, however, as they can be connected to alternate platforms as modular actuator units serially through standardized connections that extend and connect the electrical and pneumatic supply lines. In this general architecture, only a single control signal line and a single pneumatic supply line are required for connecting and controlling multiple modules in a shared system. This greatly simplifies the task of designing robotic pneumagami systems with high DoFs. This design aspect yields capabilities that have not previously been possible to exploit. At the system architecture level, it is possible to leverage extrinsic compliance in order to better match the RoM and workspace of diverse and complex applications that may be beneficial in wearable devices for daily assistance activities. At the component level, the compliance of the intrinsically soft pouch actuators used to power each module complements the high-DoF flexibility enabled by actuator modularity, allowing further benefit for interactive applications.

The unique architecture and composition of pneumagami modules introduces a new holistic design methodology complemented by novel manufacturing processes. These manufacturing and integration methods allow fully integrated functional robotic assemblies that require minimal or no additional effort to assemble and operate. The current prototype presented demonstrates several examples of this approach by incorporating features that have not been shown before in pneumatically powered robotic origami, including built in pneumatic channels, layer manufactured kinematic structure, an embedded PCB layer, and a functional passive relay valve all manufactured following 2D origami-inspired fabrication techniques. The prototype still requires some manual assembly at this stage, owing to the fact that certain functional components are not designed for layer fabrication. Future work will aim to develop or integrate new types of smaller or layer fabricated embedded control valves, perhaps powered by smart materials such as SMAs or dielectric elastomer actuators (DEAs), and incorporate pouch SPAs directly into the 2D structure during fabrication. In addition, the design and control strategy

implemented here leveraging passive control components could be readily extended to new applications that also utilize pneumatic power, beyond pneumagami-type modules or systems.

Although the context and motivation for the pneumagami module design is presented in terms of specific final applications, which include a multi-module, wearable robotic assembly, the aim in this current work is not to demonstrate these configurations in a final system but rather offer technology and background analysis to support it. Indeed, both the development and integration of multi-module systems, as well as the development of wearable interfaces (physical hardware and control-wise) requires considerable future effort, however, these challenges are seen to be subsequent to this primary introduction of the core components and techniques needed to produce pneumagami-based systems. This work helps to establish these core, critical features that are addressed systematically in preparation for future work to verify and study the performance at the full-system and application level.

The fully integrated structure of pneumagami modules fabricated from lightweight, low-form-factor materials and components facilitate highly compact robotic structures. In wearable applications for task assistance in daily activities, this feature is beneficial as it allows long duration or continuous wearability either during operational use, or between uses. Ideally, such a system would be worn on the body throughout a given day, and deployable only when needed. Subsequently, a pneumagami-based assembly could be stored when not in use without significantly impeding other activities in its compact state owing to its minimal size and weight.



5. Conclusion

A single 3-DoF pneumagami module is presented and characterized to establish the baseline performance and properties of a fully integrated hybrid robotic system combining pneumatic actuation and origami design methods. The inherently low weight and compact form factor traits common to both soft actuators and origami robots enable a space and weight efficient robotic platform that does not sacrifice strength, high mobility, or RoM. The robotic modules facilitate the construction of larger-scale, reconfigurable robotic assemblies through the use of embedded plug-and-play connection interfaces for both a shared positive pressure pneumatic supply and onboard electronics hardware. The ability to design and construct scalable robotic systems from pneumagami modules powered by inherently soft actuators consequently allows the exploitation of both the intrinsic compliance of the components themselves, as well as the effective extrinsic softness resulting from high DoFs. This design configuration affords high-RoM systems that maintain controllability and independently prescribed compliance, conducive to safety in wearable and human-robot interactive applications.

Funding

The author(s) disclosed receipt of the following financial support for the research, authorship, and/or publication of this article: This work was supported by the Swiss National Science Foundation (SNSF) and the National Centre of Competence in Research (NCCR) Robotics (Switzerland).

ORCID iDs

Matthew A Robertson  <https://orcid.org/0000-0002-2778-7232>
Ozdemir Can Kara  <https://orcid.org/0000-0003-3717-2570>

References

- Ahmed S, Ounaies Z and Frecker M (2014) Investigating the performance and properties of dielectric elastomer actuators as a potential means to actuate origami structures. *Smart Materials and Structures* 23(9): 094003.
- Al-Fahaam H, Davis S and Nefti-Meziani S (2016) Power assistive and rehabilitation wearable robot based on pneumatic soft actuators. In: *2016 21st International Conference on Methods and Models in Automation and Robotics (MMAR)*, pp. 472–477.
- Belke CH and Paik J (2017) Mori: A modular origami robot. *IEEE/ASME Transactions on Mechatronics* 22(5): 2153–2164.
- Camarillo DB, Carlson CR and Salisbury JK (2009) Configuration tracking for continuum manipulators with coupled tendon drive. *IEEE Transactions on Robotics* 25(4): 798–808.
- Cianchetti M, Follador M, Mazzolai B, Dario P and Laschi C (2012) Design and development of a soft robotic octopus arm exploiting embodied intelligence. In: *2012 IEEE International Conference on Robotics and Automation (ICRA)*. IEEE, pp. 5271–5276.
- Davenport C, Parietti F and Asada HH (2012) Design and biomechanical analysis of supernumerary robotic limbs. In: *ASME 2012 5th Annual Dynamic Systems and Control Conference Joint with the JSME 2012 11th Motion and Vibration Conference*. American Society of Mechanical Engineers, pp. 787–793.
- Fang H, Fang Y and Zhang K (2013) Kinematics and workspace analysis of a novel 3-DOF parallel manipulator with virtual symmetric plane. *Proceedings of the Institution of Mechanical Engineers, Part C: Journal of Mechanical Engineering Science* 227(3): 620–629.
- Felton S, Becker K, Aukes D and Wood R (2015) Self-folding with shape memory composites at the millimeter scale. *Journal of Micromechanics and Microengineering* 25(8): 085004.
- Felton S, Tolley M, Demaine E, Rus D and Wood R (2014) A method for building self-folding machines. *Science* 345(6197): 644–646.
- Firouzeh A and Paik J (2015) Robogami: A fully integrated low-profile robotic origami. *Journal of Mechanisms and Robotics* 7(2): 021009.
- Firouzeh A and Paik J (2017) An under-actuated origami gripper with adjustable stiffness joints for multiple grasp modes. *Smart Materials and Structures* 26(5): 055035.
- Ge Q, Dunn CK, Qi HJ and Dunn ML (2014) Active origami by 4D printing. *Smart Materials and Structures* 23(9): 094007.
- Huo W, Mohammed S, Moreno JC and Amirat Y (2016) Lower limb wearable robots for assistance and rehabilitation: A state of the art. *IEEE Systems Journal* 10(3): 1068–1081.

- In H, Kang BB, Sin M and Cho K (2015) Exo-Glove: A wearable robot for the hand with a soft tendon routing system. *IEEE Robotics Automation Magazine* 22(1): 97–105.
- Kim SJ, Lee DY, Jung GP and Cho KJ (2018) An origami-inspired, self-locking robotic arm that can be folded flat. *Science Robotics* 3(16): eaar2915.
- Kurumaya S, Nabae H, Endo G and Suzumori K (2018) Exoskeleton inflatable robotic arm with thin McKibben muscle. In: *2018 IEEE International Conference on Soft Robotics (RoboSoft)*. IEEE, pp. 120–125.
- Lee DY, Jung GP, Sin MK, Ahn SH and Cho KJ (2013) Deformable wheel robot based on origami structure. In: *2013 IEEE International Conference on Robotics and Automation (ICRA)*. IEEE, pp. 5612–5617.
- Liang X, Cheong H, Sun Y, Guo J, Chui CK and Yeow CH (2018) Design, characterization, and implementation of a two-dof fabric-based soft robotic arm. *IEEE Robotics and Automation Letters* 3(3): 2702–2709.
- Liu T, Wang Y and Lee K (2018) Three-dimensional printable origami twisted tower: Design, fabrication, and robot embodiment. *IEEE Robotics and Automation Letters* 3(1): 116–123.
- McClintock H, Temel FZ, Doshi N, Koh Js and Wood RJ (2018) The milliDelta: A high-bandwidth, high-precision, millimeter-scale Delta robot. *Science Robotics* 3(14): eaar3018.
- McMahan W, Jones BA and Walker ID (2005) Design and implementation of a multi-section continuum robot: Air-octor. In: *IROS*, pp. 2578–2585.
- Mintchev S, Shintake J and Floreano D (2018) Bioinspired dual-stiffness origami. *Science Robotics* 3(20): eaau0275.
- Miyashita S, Guitron S, Luidersdorfer M, Sung CR and Rus D (2015) An untethered miniature origami robot that self-folds, walks, swims, and degrades. In: *2015 IEEE International Conference on Robotics and Automation (ICRA)*. IEEE, pp. 1490–1496.
- Mu J, Hou C, Wang H, Li Y, Zhang Q and Zhu M (2015) Origami-inspired active graphene-based paper for programmable instant self-folding walking devices. *Science Advances* 1(10): e1500533.
- Na JH, Evans AA, Bae J, et al. (2015) Programming reversibly self-folding origami with micropatterned photo-crosslinkable polymer trilayers. *Advanced Materials* 27(1): 79–85.
- Nguyen PH, Sparks C, Nuthi SG, Vale NM and Polygerinos P (2019) Soft poly-limbs: Toward a new paradigm of mobile manipulation for daily living tasks. *Soft Robotics* 6(1): 38–53.
- Niiyama R, Rus D and Kim S (2014) Pouch motors: Printable/inflatable soft actuators for robotics. In: *2014 IEEE International Conference on Robotics and Automation (ICRA)*. IEEE, pp. 6332–6337.
- Onal CD, Wood RJ and Rus D (2011) Towards printable robotics: Origami-inspired planar fabrication of three-dimensional mechanisms. In: *2011 IEEE International Conference on Robotics and Automation (ICRA)*. IEEE, pp. 4608–4613.
- Onal CD, Wood RJ and Rus D (2013) An origami-inspired approach to worm robots. *IEEE/ASME Transactions on Mechatronics* 18(2): 430–438.
- Paik JK, Byoungkwon A, Rus D and Wood RJ (2012) Robotic origamis: Self-morphing modular robot. In: *Proceedings of the 2nd International Conference on Morphological Computation ICMC, EPFL-CONF-206919*, Venice, 2012.
- Polygerinos P, Correll N, Morin SA, et al. (2017) Soft Robotics: Review of fluid-driven intrinsically soft devices; manufacturing, sensing, control, and applications in human–robot interaction. *Advanced Engineering Materials* 19(12): 1700016.
- Polygerinos P, Wang Z, Galloway KC, Wood RJ and Walsh CJ (2015) Soft robotic glove for combined assistance and at-home rehabilitation. *Robotics and Autonomous Systems* 73: 135–143.
- Qi R, Khajepour A, Melek WW, Lam TL and Xu Y (2017) Design, kinematics, and control of a multijoint soft inflatable arm for human-safe interaction. *IEEE Transactions on Robotics* 33(3): 594–609.
- Renda F, Giorelli M, Calisti M, Cianchetti M and Laschi C (2014) Dynamic model of a multibending soft robot arm driven by cables. *IEEE Transactions on Robotics* 30(5): 1109–1122.
- Robertson MA and Paik J (2016) Trunk postural tracking of assistive soft pneumatic actuator belt. In: *Dynamic Walking Conference*, Holly, MI, 2016.
- Robertson MA and Paik J (2017) New soft robots really suck: Vacuum-powered systems empower diverse capabilities. *Science Robotics* 2(9): eaan6357.
- Robertson MA, Sadeghi H, Florez JM and Paik J (2017) Soft pneumatic actuator fascicles for high force and reliability. *Soft Robotics* 4(1): 23–32.
- Rodriguez Leal E and Dai JS (2007) From origami to a new class of centralized 3-DOF parallel mechanisms. In: *ASME 2007 International Design Engineering Technical Conferences and Computers and Information in Engineering Conference*, pp. 1183–1193.
- Rus D and Tolley MT (2018) Design, fabrication and control of origami robots. *Nature Reviews Materials* 3(6): 101.
- Salerno M, Firouzeh A and Paik J (2017) A low profile electromagnetic actuator design and model for an origami parallel platform. *Journal of Mechanisms and Robotics* 9(4): 041005.
- Salerno M, Zhang K, Menciassi A and Dai JS (2016) A novel 4-DOF origami grasper with an SMA-actuation system for minimally invasive surgery. *IEEE Transactions on Robotics* 32(3): 484–498.
- Santoso J, Skorina EH, Luo M, Yan R and Onal CD (2017) Design and analysis of an origami continuum manipulation module with torsional strength. In: *2017 IEEE/RSJ International Conference on Intelligent Robots and Systems (IROS)*, pp. 2098–2104.
- Tolley MT, Felton SM, Miyashita S, Aukes D, Rus D and Wood RJ (2014) Self-folding origami: Shape memory composites activated by uniform heating. *Smart Materials and Structures* 23(9): 094006.
- Tolley MT, Felton SM, Miyashita S, et al. (2013) Self-folding shape memory laminates for automated fabrication. In: *2013 IEEE/RSJ International Conference on Intelligent Robots and Systems (IROS)*. IEEE, pp. 4931–4936.
- Vander Hoff E, Jeong D and Lee K (2014) Origamibot-i: A thread-actuated origami robot for manipulation and locomotion. In: *2014 IEEE/RSJ International Conference on Intelligent Robots and Systems (IROS 2014)*. IEEE, pp. 1421–1426.
- Vatsal V and Hoffman G (2017) Wearing your arm on your sleeve: Studying usage contexts for a wearable robotic forearm. In: *2017 26th IEEE International Symposium on Robot and Human Interactive Communication (RO-MAN)*. IEEE, pp. 974–980.

- Yang H, Xu M, Li W and Zhang S (2018) Design and implementation of a soft robotic arm driven by SMA coils. *IEEE Transactions on Industrial Electronics* 66(8): 6108–6116.
- Zhakypov Z, Falahi M, Shah M and Paik J (2015) The design and control of the multi-modal locomotion origami robot, Tribot. In: *2015 IEEE/RSJ International Conference on Intelligent Robots and Systems (IROS)*, pp. 4349–4355.
- Zhakypov Z, Heremans F, Billard A and Paik J (2018) An origami-inspired reconfigurable suction gripper for picking objects with variable shape and size. *IEEE Robotics and Automation Letters* 3(4): 2894–2901.
- Zhang K, Qiu C and Dai JS (2016) An extensible continuum robot with integrated origami parallel modules. *Journal of Mechanisms and Robotics* 8(3): 031010.